Journal of Asian Earth Sciences 173 (2019) 113–120

Contents lists available at ScienceDirect

Journal of Asian Earth Sciences

journal homepage: www.elsevier.com/locate/jseaes

# Seismotectonic characteristics of the Taiwan collision-Manila subduction transition: The effect of pre-existing structures

Shao-Jinn Chin[a,b], Jing-Yi Lin[a,b,*], Yi-Ching Yeh[a], Hao Kuo-Chen[a], Chin-Wei Liang[b]

[a] Department of Earth Sciences, National Central University, No. 300, Jhongda Rd., Jhongli City, Taoyuan 32001, Taiwan, ROC
[b] Center for Environmental Studies, National Central University, No. 300, Jhongda Rd., Jhongli City, Taoyuan 32001, Taiwan, ROC

ARTICLE INFO

*Keywords:*
Collision
Subduction
Taiwan
Manila
Ocean bottom seismometer
Passive margin

ABSTRACT

Based on the distribution of an earthquake swarm determined from an ocean bottom seismometer (OBS) network deployed from 20 August to 5 September 2015 in the northernmost part of the South China Sea (SCS) and data from inland seismic stations in Taiwan, we resolved a $M_L$ 4.1 earthquake occurring on 1 September 2015 as a NE-SW-trending left-lateral strike-slip event that ruptured along the pre-existing normal faults generated during the SCS opening phases. The direction of the T-axes derived from the $M_L$ 4.1 earthquake and the background seismicity off SW Taiwan present high consistency, indicating a stable dominant NW-SE tensional stress for the subducted Eurasian Plate (EUP). The distinct stress variations on the two sides of these reactivated NE-SW trending features suggest that the presence of pre-existing normal faults and other related processes may lessen the lateral resistance between the Taiwan collision and Manila subduction system, and facilitate the slab-pull process for the subducting portion, which may explain the NW-SE tensional stress environment near the transition boundary in the northernmost part of the SCS.

## 1. Introduction

Generally, different tectonic environments can be characterized by distinct seismogenic behaviors, such as extensional mechanisms at mid-ocean ridges and underthrusting earthquakes along subduction systems. However, when several important tectonic procedures are interwoven, seismic activity is complicated and indiscernible. Located near the northernmost tip of the South China Sea (SCS), western Taiwan and its SW offshore are withstanding the arc-continental collision to the north, which forms the Taiwan orogen (Fig. 1), and the subduction process to the south, which constitutes the Manila subduction zone. The transition between collision and subduction is suggested to occur near the SW Taiwan offshore area (Kao et al., 2000; Liu et al., 2004; Shyu et al., 2005) where the obvious bathymetric morphology reveals the presence of a passive margin. Along this convergent belt, compressional stress subparallel to the plate motion or the trench-normal direction should dominate the regional seismicity. However, various seismogenic characteristics appear along this collision-subduction system (Hsu et al., 2009; Liao et al., 2008; Rau et al., 2012; Wu et al., 2009; Yang et al., 2016), including high- and low-angle compression, trench-parallel and trench-perpendicular extension and strike-slip effects. On the other hand, pre-existing structures inherited from ancient continental rifting process and changes in the nature of the lithosphere are thought to affect the seismogenic signature (Bent, 2002; Talwani and Rajendran, 1991). Although rifting-related normal faults originating from the SCS opening are widespread off SW Taiwan (Lester et al., 2014; McIntosh et al., 2013; Yang et al., 2006; Yeh et al., 2012), and are positively involved in the Taiwan orogeny (Rau et al., 2012), their influences on the offshore Taiwan seismogenic structures and the collision-subduction process remain questionable. However, only a few moderate to large earthquakes have been recorded near the area in the past decades. Conducting relevant discussions is difficult due to the lack of micro-seismic records for offshore SW Taiwan. In this study, with the deployment of an ocean bottom seismometer (OBS) network, we collected information for a $M_L$ 4.1 earthquake and its related swarm occurring off SW Taiwan, which is generally considered to be a seismically inactive area. The combination of the OBS and the Central Weather Bureau (CWB) inland station data enables a better hypocenters localization and the determination of the focal mechanism for the $M_L$ 4.1 event. By combining the regional seismicity distribution, the slab geometry and the stress expression, we aim to discern the seismogenic environment along this Taiwan collision-Manila subduction system, which could be valuable for the estimation of tsunami and shaking hazards in Southeast Asia.

* Corresponding author at: Department of Earth Sciences, National Central University, Taiwan, ROC.
*E-mail address:* jylin@ncu.edu.tw (J.-Y. Lin).

https://doi.org/10.1016/j.jseaes.2019.01.014
Received 3 September 2018; Received in revised form 7 January 2019; Accepted 8 January 2019
Available online 17 January 2019
1367-9120/ 

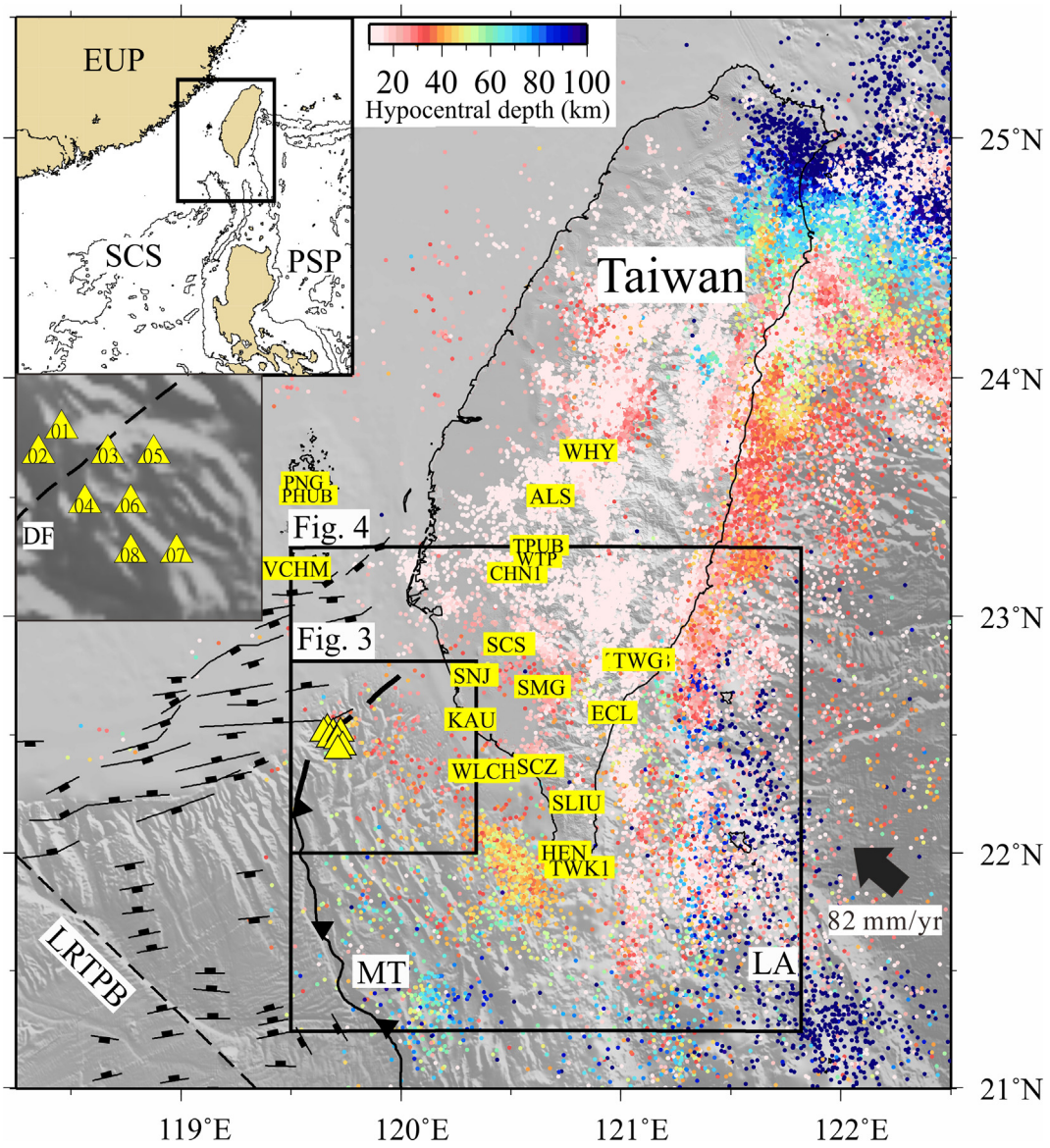


**Fig. 1.** Tectonic map and earthquake distribution of the northern-most South China Sea (SCS) and Taiwan orogen. Colored dots are earthquakes with $M_L > 3$ (Wu et al., 2008, catalog updated until 2016); normal faults off SW Taiwan are modified from Yang et al. (2006) and Yeh et al. (2012). The black arrow represents the plate motion of the Philippine Sea Plate relative to the Eurasian Plate. Abbreviations in yellow rectangles represent the inland Central Weather Bureau (CWB) seismic stations used in this study. The two insets show the regional tectonics of the study area and the enlarged map for the distribution of the eight ocean bottom seismometers (OBSs). Yellow triangles show the OBSs. DF: Deformation front; EUP: Eurasian Plate; LA: Luzon Arc; LRTPB: Luzon-Ryukyu Transition Plate Boundary; MT: Manila Trench; PSP: Philippine Sea Plate; SCS: South China Sea. (For interpretation of the references to colour in this figure legend, the reader is referred to the web version of this article.)

## 2. Tectonic setting

The active Taiwan orogen originating from arc-continent collision between the Eurasian Plate (EUP) and the Philippine Sea Plate (PSP) began approximately 5–6 Ma (Teng, 1990; Tsai et al., 1977). The rapid convergence rates of 7 and 8.2 cm/yr revealed by plate reconstruction (Seno et al., 1993) and geodetic analyses (Hsu et al., 2009; Yu et al., 1997), respectively, suggest an ongoing mountain building process in the present. Due to the oblique convergence between the two plates, the orogeny in the island propagates from north to south (Suppe, 1984). Onshore and offshore southern Taiwan, where the EUP subducts eastward beneath the PSP along the Manila Trench, are in an initial stage of collision (Huang et al., 1997; Kao et al., 2000; Reed et al., 1992).

The subducting oceanic crust in the SCS initially broke ~32 Ma based on the interpretation of marine magnetic lineations (Briais et al., 1993; Taylor and Hayes, 1983). Given a northeast-trending magnetic anomaly pattern, Hsu et al. (2004) interpreted an earlier stage of sea floor spreading occurring ~37 Ma, which is bounded by the Luzon–Ryukyu transform plate boundary (LRTPB) to its east. The two sides of the LRTPB exhibit different tectonic environments. A relatively thicker oceanic crust exists to the west, whereas a rifted continental crust to the east (McIntosh et al., 2013). Based on seismic reflection data, numerous normal faults, covered by *syn*-rift strata and postrift sediments, have been mapped for the entire northeastern portion of the SCS. Most of these faults cut through the upper crust, connecting from the seafloor to the detachment above the lower crust, or even down to the Moho (Lester et al., 2014; McIntosh et al., 2014; Yeh et al., 2012).

Since the area between the northernmost Manila subduction zone and southern Taiwan is considered a transition from subduction to initial collision, previous works have used available seismological and geological data to obtain a better understanding of the boundary and the tectonic processes occurring in the vicinity of this transition (e.g.,

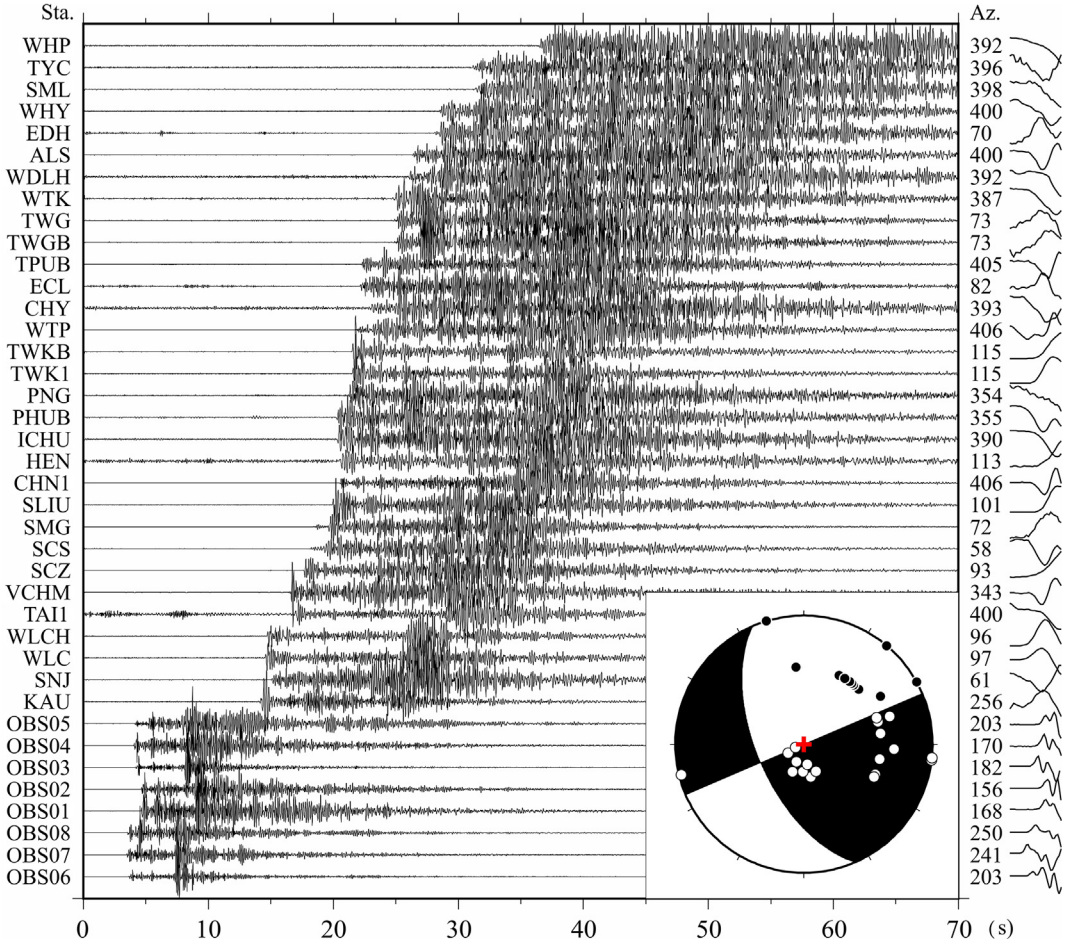


**Fig. 2.** Vertical component waveforms recorded by the OBSs and inland stations and the focal mechanism of the 2015 $M_L$ 4.1 earthquake. Station codes are shown in left panel; the azimuths and polarities of first arrivals are shown in the right panel.

Eakin et al., 2014; Huang et al., 2004; Liu et al., 1997; 2004; Yu, 2004). By using focal mechanisms, Kao et al. (2000) illustrated a clear Wadati-Benioff zone to the south of 21.5°N. However, along with a lack of subduction-related seismicity, the Manila Trench loses its bathymetric definition north of 21.5°N, and its tectonic identity becomes unclear. The connection between a typical collision zone and a subduction area is the so-called deformation front (DF). The DF extends NNW from the northern edge of the Manila Trench to the foot of the continental slope, and progressively turns to a NNE-SSW direction before it enters inland Taiwan and connects to the mountain belt (Fig. 1). By analogy with the geological context of the Nankai Trough area in Japan, Lin et al. (2009) suggested a high seismogenic potential along the plate interface and out-of-sequence thrusts of the Manila subduction system. However, Lin et al. (2015) showed a wide distribution of extensional earthquakes along the trench and its neighboring areas, which suggests that the plates are in a relaxed state instead of accumulating tectonic stress. In fact, in contrast with the high strain rate distribution (Yu et al., 1997), only a few moderate to large earthquakes have been recorded near the transition area (along the DF) in the past decades (Wu et al., 2008). The largest recent seismic events off SW Taiwan are the Pingtung doublet earthquakes that occurred on 26 December 2006. The regional tomographic result shows that the two $M_L$ 7.0 earthquakes should have occurred in and/or beneath the subducted slab rather than along the plate interface (Chen et al., 2008; Liao et al., 2008; Wu et al., 2009).

## 3. Data from the OBS network

Eight OBSs were deployed offshore southwestern Taiwan from 20 August to 5 September 2015 with a small spacing of 3.3–10.8 km (inset in Fig. 1). This OBS network was originally designed to monitor the ground motion around some degassing spots located in the continental slope of the NE tip of the SCS. However, the occurrence of the 1 September 2015, $M_L$ 4.1 earthquake makes the network the best device to further investigate the tectonic environment of this relatively inactive seismic area. MicrOBS, the OBS we used in this study was developed by the French Research Institute for Exploitation of the Sea (Ifremer) (Auffret et al., 2004). Each MicrOBS contains one hydrophone and three orthogonal 4.5 Hz geophones as receivers and records data with a sampling rate of 125 Hz. The P- and S-wave arrivals in the OBS records were determined initially with the STA/LTA method (Allen, 1982) and then checked manually. To obtain better ray-path coverage, the seismic arrivals determined from the OBS records were integrated with those of the CWB catalog based on the following criteria: (1) the difference in epicenter should be less than 0.1°in both latitude and longitude; (2) the difference in origin time should be less than 30 s. The CWB network is capable of determining earthquakes as small as $M_L$ 1. When no event appears in the CWB catalog, the earthquake signal is usually mixed with the background noise and the arrivals are not easy to determine. Thus, the use of the CWB catalog should be sufficient for the present study. However, the focal depth determined from the CWB catalog is not a concern due to the large uncertainty possibly caused by the poor station coverage of each individual network and the indefinite velocity model. Fig. 2 shows the waveforms of the 2015 $M_L$ 4.1 earthquake recorded by both the OBSs and inland seismic stations. Based on the 17-day OBS data, a total of 114 earthquakes, containing 595 P- and 659 S-wave arrivals were selected. As we do not have an appropriate regional 3-D

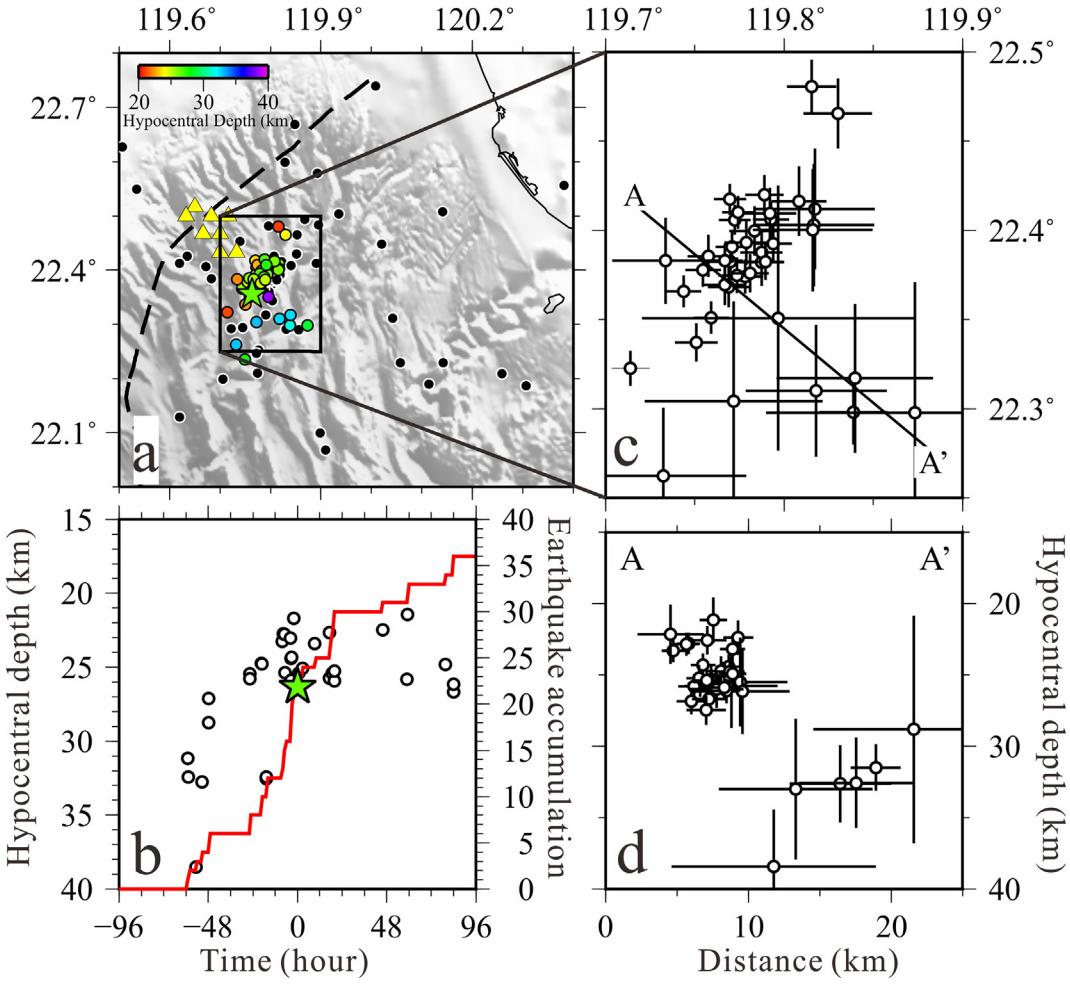


**Fig. 3.** (a) Map view of the earthquake swarm for the 2015 $M_L$ 4.1 earthquake series before and after relocation. Colored dots indicate relocated events, whereas black dots are events that were excluded from the relocation. The green star shows the $M_L$ 4.1 mainshock and the yellow triangles represent the OBSs. The dashed line shows the DF. (b) Temporal distribution of the 2015 $M_L$ 4.1 earthquake series with regard to the main shock. Most fore/aftershocks occurred within 24 h before and after the mainshock. The green star shows the $M_L$ 4.1 mainshock and the hollow circles represent the fore/aftershocks. (c) Enlarged map in plain view of the relocated earthquakes with location errors. The area is shown in (a). (d) The distribution and location errors of the relocated earthquakes along the NW-SE-trending AA' profile indicated in (c). (For interpretation of the references to colour in this figure legend, the reader is referred to the web version of this article.)

tomographic velocity model, the hypocenter of these events was determined first with the global velocity model iasp91 (Kennett and Engdahl, 1991). Then, the 727 P- and 592 S-wave arrivals extracted from the CWB catalog were added to perform an earthquake relocation procedure. We relocated the earthquakes by using the double-difference relocation method (HypoDD, Waldhauser and Ellsworth, 2000) to minimize the effect of the velocity model and clock bias. The waveform cross-correlation method was not applied to define event pairs because of the relatively low signal-to-noise level of OBS data and the uncertainty in the orientation of the three components of the geophones. Finally, a group of 41 earthquakes, aligning along a NE-SW-trending seismic zone with an almost vertical distribution, was illustrated with an average depth of approximately 25 km (colored dots in Fig. 3a). Seventy-three events were discarded from our dataset because they were located too far from the target area and too scattered to be relocated with the double-difference relocation method. As shown by the black dots in Fig. 3a, when an earthquake is far from its neighboring event and outside the seismic networks, this earthquake is excluded from the relocation process. Fig. 3c and d show the location error in map view and along a profile AA'. Most earthquakes have a location error of less than several kilometers in both the horizontal and vertical directions, indicating a reliable seismic pattern after the relocation. The origin times of most events appeared within 24 h before or after the $M_L$ 4.1 mainshock (Fig. 3b). The original location of the 2015 $M_L$ 4.1 earthquake, reported by the CWB, was 119.71°E, 22.44°N, and 48.3 km deep. Integration of the data from the two seismic networks and the earthquake relocation result in a new hypocenter for the $M_L$ 4.1 event, which is 119.76°E, 22.38°N, and 26.3 km deep. A relatively minor horizontal displacement and a larger focal depth variation are observed after the relocation. The new hypocenter is obviously shallower than that in the CWB catalog. This large discrepancy in focal depth should have resulted from the different coverage of seismic stations and the relatively simple velocity model used for routine location in the CWB. Therefore, the focal depth obtained by combining arrivals from OBS and inland stations and applying the HypoDD relocation method should be more reliable. In addition, the OBSs and the CWB inland stations together provide the polarity of the first motion from different azimuths and enable the determination of a reliable focal mechanism (Fig. 2).

## 4. Results and discussion

### 4.1. Origin of the 2015 $M_L$ 4.1 earthquake off SW Taiwan

The 2015 $M_L$ 4.1 earthquake cluster shows a NE-SW trending pattern with a subvertical distribution pattern. The focal mechanism solution of the mainshock also defines two fault planes of strike-slip type

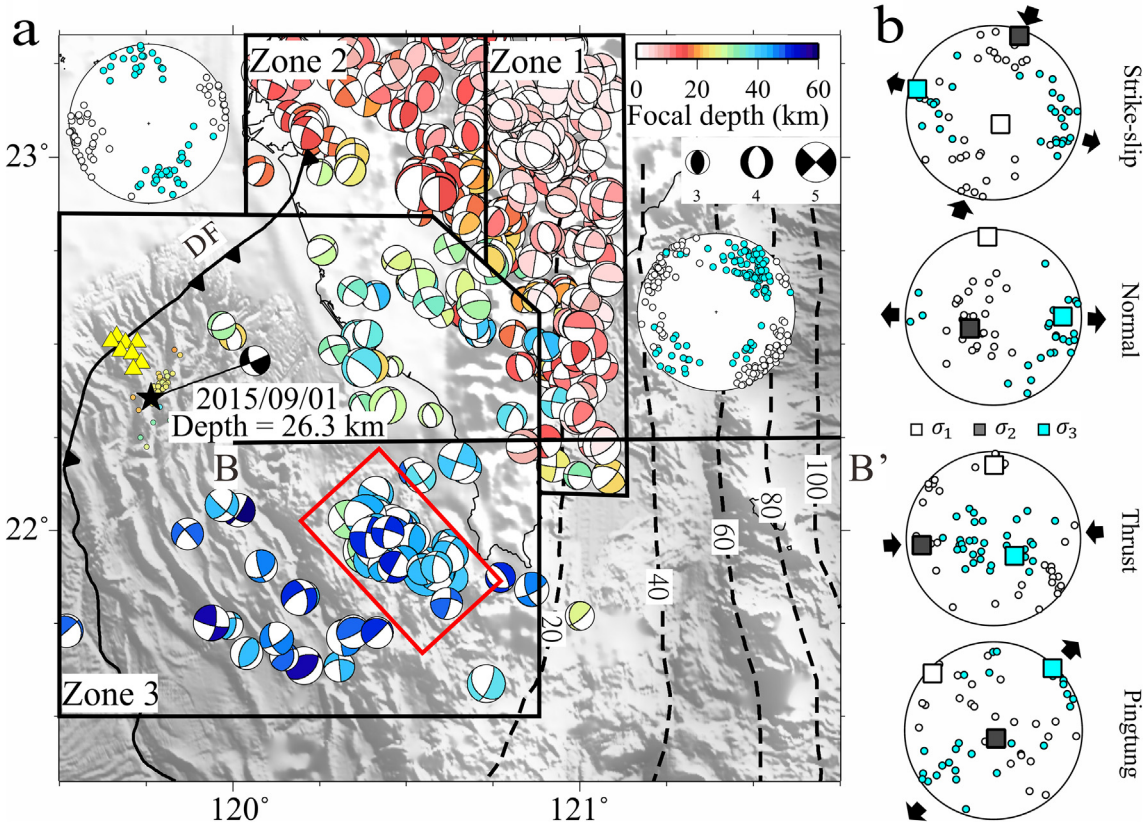


**Fig. 4.** (a) Focal mechanism solutions ($M_L$ > 4) in the SW Taiwan area from Wu et al. (2008, update until 2016) and the Broadband Array in Taiwan for Seismology (BATS) (Institute of Earth Sciences, Academia Sinica, Taiwan, 1996). Colors represent the different depths. To prevent the influence of other geological structures in our interpretation, only the earthquakes located west of 121.3°E are shown. The black star and beach ball show the 2015 $M_L$ 4.1 mainshock. The yellow triangles are the OBSs. The three thick black blocks and red rectangles indicate the zones where we performed the stress analysis. The P- and T-axes distribution of Zone 1 and Zone 2 are plotted in its vicinity. Dashed lines are contours of the plate interface mapped from the velocity model and seismicity. The number on the dashed line indicates the depth of slab isobaths in km. (b) P- and T-axes of different types of earthquakes derived from the focal mechanisms of the Zone 3 area in (a). Earthquakes in the Pingtung doublet area are evaluated independently. White and light blue dots show the P- and T-axes, respectively. White, gray and light blue squares in (b) indicate the inverted $\sigma_1$, $\sigma_2$ and $\sigma_3$, respectively. (For interpretation of the references to colour in this figure legend, the reader is referred to the web version of this article.)

with a large dip angle. Considering both the hypocentral distribution and the two best-fitting fault planes, we suggest that the $M_L$ 4.1 earthquake was a sinistral strike-slip event, rupturing along the NE-SW direction focal plane with 246.67°, 89°, 30° for strike, dip, and rake, respectively (Fig. 2). Based on the seismic reflection and refraction data obtained in the northern part of the SCS, the crustal thickness was determined to lie between 9 and 15 km (Lester et al., 2014; Yeh et al., 2012; Zhao et al., 2010). This crustal thickness variation off SW Taiwan reflects a transition from an oceanic to a rifted continental lithosphere, which is the general structural trait of a passive margin. As the focal depth of the $M_L$ 4.1 earthquake is defined as 26.3 km and the average depth of the cluster is approximately 25 km, we suggest that this $M_L$ 4.1 earthquake and its fore- and after-shocks should have occurred in the subducted EUP. This interpretation means that any geological features, existing in the subducted plate with high dip angles should be candidates to have caused the $M_L$ 4.1 earthquake series. In the collision-subduction area, most seismic activity occurs in the crustal portion, in the upper (overriding) plate or along the plate interface (e.g., Chin et al., 2016). The most likely candidate structures for occurrence of the $M_L$ 4.1 earthquake would be the widespread pre-existing normal faults in the subducted oceanic plate. Along the entire continental margin off SW Taiwan, a large number of normal faults resulting from the SCS rifting phase truncate the basement and constitute the main crustal features (Lester et al., 2014; Yeh et al., 2012). Most of these faults have consistent strikes of approximately E-W or NE-SW (Liu et al., 1997; 2004; Yeh et al., 2012) (Fig. 1), which is subparallel not only to the fault plane revealed by the earthquake swarm observed in our study but also to one of the nodal planes of the historical strike-slip earthquakes that have occurred in the subducted plate (Fig. 4a). Consequently, we suggest that the 2015 $M_L$ 4.1 earthquake series should have ruptured along one of these pre-existing normal faults.

### 4.2. Dominant stress regime off SW Taiwan

To understand the dynamic force of the tectonic environment off SW Taiwan, we analyzed the distribution of the compressional axis (P-axis) and the tensional axis (T-axis) derived from the available focal mechanism solutions in this area (Fig. 4). The databases used include the published data of Wu et al. (2008; 2010, updated until 2016) and those provided by the Broadband Array in Taiwan for Seismology (BATS) (Institute of Earth Sciences, Academia Sinica, Taiwan, 1996). The accuracy of earthquake hypocenter determination is important when analyzing tectonic structures. Therefore, we principally used the focal mechanism parameters of Wu et al. (2008, 2010, updated until 2016), which relocated the earthquakes by incorporating a large dataset and adopting a 3-D velocity model. Although the dataset was published in 2008, the catalog has been systematically updated until 2016. On the other hand, in order to make the best use of all the available data, we also completed our stress analysis by using the BATS catalog. Events located east of 121°E are not discussed to avoid the possible influence of other geological units, such as the Luzon Arc (Figs. 1 and 4a). In order to define the subducted and overriding plate, we determined the

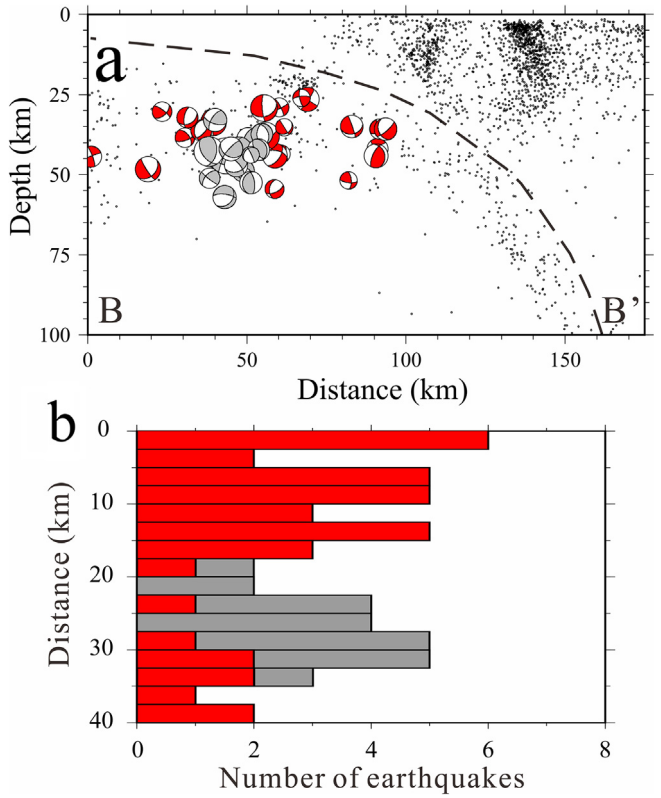


**Fig. 5.** (a) Background seismicity and focal mechanism distribution along the E-W BB' profile shown in Fig. 4a. Red and gray focal mechanisms represent the events used for the estimation of P- and T-axes for the Zone 3 area in Fig. 4a and the 2006 Pingtung doublet earthquake area, respectively. The black dots show the background seismicity from Wu et al. (2008, catalog updated until 2016). The dashed line is the plate interface determined from the velocity model of McIntosh et al. (2013) and the background seismicity. (b) Number of earthquakes versus the distance with regard to the top of the subducted plate plotted in (a). Gray and red bars show the number of events calculated from the earthquakes in and outside the 2006 Pingtung doublet earthquake area. (For interpretation of the references to colour in this figure legend, the reader is referred to the web version of this article.)

plate interface based on the tomographic velocity model (Kuochen et al., 2012), seismic refraction data (McIntosh et al., 2013) and seismicity distribution (Figs. 4a and 5a). The seismicity can be visibly divided into two groups by the plate interface. The earthquakes located above the interface occur in the overriding plate (Zone 1 and Zone 2 in Fig. 4a), while those beneath the interface occur in the subducted plate (Zone 3 in Fig. 4a). The depth of the plate interface is shallower than approximately 25 km in our study area (Zone 3 in Fig. 4a), and the focal mechanisms of the area are located beneath 25 km, in the subducted plate (Fig. 5a). Thus, the analysis we performed should express the stress state of the subducting lithosphere. Furthermore, most earthquakes with depths shallower than 25 km occur to the north of the DF and its prolongation (~23°N), whereas those with depth deeper than 25 km are observed only to its south (Fig. 4a). This boundary, the DF and its prolongation, trending NE-SW off SW Taiwan, has been mapped along the border of the continental slope, where one of the major pre-existing normal faults is located (Fig. 1). The different earthquake distributions on its two sides could indicate the distinct seismogenic environments. Visual examination also shows that the P-axes of the shallow depth events exhibit a stable ~NW-SE direction in eastern Taiwan (Zone 1 in Fig. 4a) and then turn to an ~E-W direction in the western part (Zone 2 in Fig. 4a), which reflects the convergence direction between the two plates. However, the variations in the P-axes of the earthquakes deeper than 25 km present a different pattern (Zone 3 in Fig. 4a). To the west of 121°E, although the thrust type earthquakes still possess ~E-W P-axes, the P-axes turn to the ~N-S direction for the strike-slip type earthquakes (Fig. 4b), which is different from the observed plate convergent direction. Based on the discernible change in the P-axis direction, we suggest that most of the Taiwanese orogen is indeed influenced mainly by the convergent system, except for the portion located to SW Taiwan, at depths deeper than 25 km, i.e., the subducted plate. Thus, the subducted plate should have a different stress environment from its surrounding area.

To further understand how the stress regime varies in the subducted plate, P- and T-axes calculated from normal, thrust, and strike-slip focal mechanisms are plotted in Fig. 4b. It is notable that the P- and T-axes for the source area of the 2006 Pingtung doublet are plotted independently because of its high spatial concentrations and its stress state distinct from that of other events. The P- and T-axis estimations from all the earthquakes show extremely scattered results, which is why we plot them individually to provide a better illustration. The result shows that only the 2006 Pingtung doublet source area contains a T-axis distribution distinct from that of the other earthquakes occurring in the subducted plate. The T-axis for the 2006 Pingtung earthquake area trends mainly along the NE-SW direction, whereas the T-axis for the other focal mechanisms shows an ~E-W direction (Fig. 4b). This ~E-W T-axis distribution is approximately subparallel to the direction of relative plate motion between the EUP and PSP (Seno et al., 1993), indicating a stress regime obviously different from the ongoing convergent process, which should have a NW-SE or E-W trending P-axis. To explain why the 2006 Pingtung doublet source area has a different T-axis direction, we calculated the vertical distance between the hypocenters and the plate interface determined from a seismic refraction tomographic model (McIntosh et al., 2013) for all the $M_L > 4$ historical earthquakes of the area (Fig. 5b) and counted the number of earthquakes with similar depths. We noticed that the majority of the earthquakes for the 2006 Pingtung doublet occurred at a distance of 20–35 km with respect to the top of the subducted plate (gray bars in Fig. 5b), whereas 0–20 km for the other background seismicity (red bars in Fig. 5b). Based on the crustal thickness (~9–15 km) of the area (Yeh et al., 2012; Zhao et al., 2010; Lester et al., 2014), the hypocenters of the 2006 Pingtung earthquakes are located in the upper mantle of the subducted lithosphere, while most of the other earthquakes were generated in the crustal portion (Fig. 5b). Therefore, it is highly possible that the 2006 Pingtung earthquakes and the other earthquakes have different natures and display different origins. The 2006 Pingtung earthquake series has been proposed to have been an intra-slab event that occurred near the bottom of the subducted lithosphere and was caused by the slab bending effect (Liao et al., 2008; Wu et al., 2009). The concentration of the hypocenters in a limited area may also indicate that the earthquake series was induced by local stress variation. If this interpretation is correct, the difference in the T-axis distribution for the 2006 Pingtung earthquakes and that of the other earthquakes could be understood, and this local stress fluctuation should not be taken into account for the general setting of the regional stress configuration. Therefore, the stress pattern of the subducted plate in SW Taiwan and its offshore portion, located in the collision-subduction transition, demonstrates a different stress regime from that of the regional convergent tectonic context.

### 4.3. Origin of the seismogenic variation in the collision-subduction transition

In the previous sections, the consistency of the earthquake distribution determined by the seismic stations and the local structures shows the reactivation of pre-existing normal faults. Furthermore, the distinct stress patterns on the two sides of the northern part of the DF, where one of the major pre-existing normal faults is located, indicates that the DF should be one of the important tectonic boundaries for the subducted plate. Therefore, the presence of pre-existing faults may

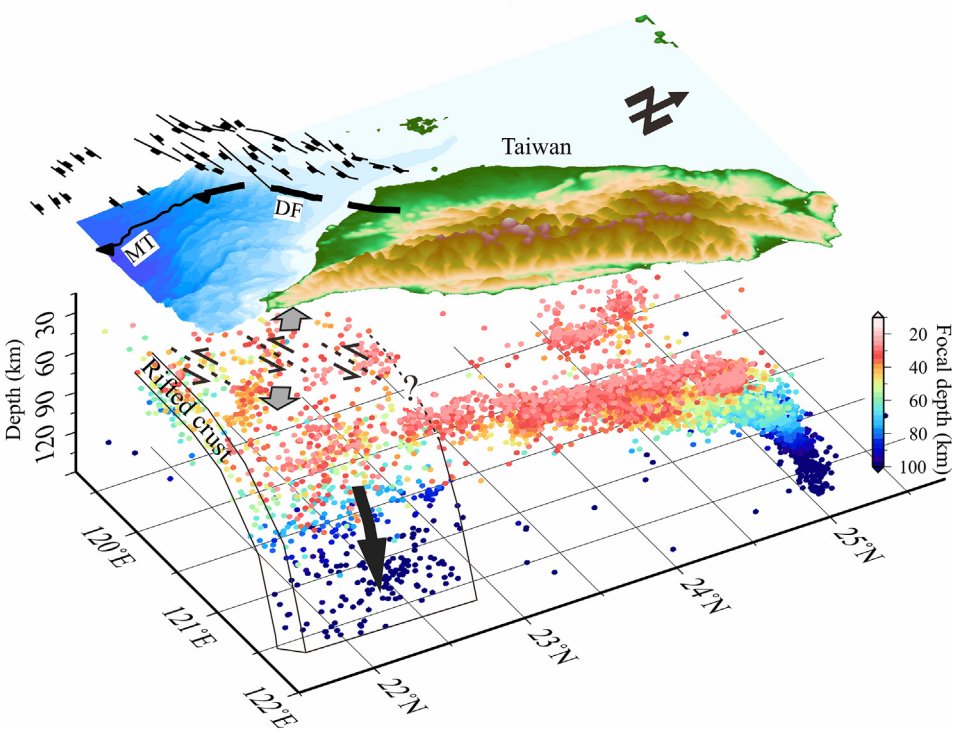


**Fig. 6.** A 3-D schematic model for the distribution of earthquakes and the possible tectonic environment in the subducted plate for the Taiwan collision-Manila subduction transition zone. Topography, pre-existing normal faults (modified from Yang et al., 2006; Yeh et al., 2012), Manila Trench and the DF are shown above the seismicity distribution, which includes earthquakes with $M_L > 3$ (Wu et al., 2008). Black and gray arrows indicate the enhanced slab pull force at depth and the tensional stress for the shallower portion due to the densification of the slab, respectively. Thin arrows and dashed lines represent strike-slip events that occurred along pre-existing faults in the subducted EUP.

promote the reduction of the connection between the collision and subduction zones and enhance the down-dip motion of the subducted portion by decreasing the lateral resistance. However, the reactivated pre-existing structures alone should not be capable of causing such significant stress variation from a dominantly NW-SE compressive stress environment to the north to a tensional regime in a similar direction to the south. A widespread distribution of serpentinized materials was inferred for the northern Manila subduction zone and southern Taiwan based on gravity anomaly modeling (Doo et al., 2015) and petrophysical analysis (Brown et al., 2015), indicating a hydrated mantle wedge and dehydrated subducted plate. On the one hand, slab dehydration could cause densification of the subducted plate material (Kirby et al., 1996), which would intensify the slab subduction process and create an extensional environment at a shallower depth. On the other hand, the presence of serpentinization at the base of the mantle wedge would decrease the coupling between the subducting and overriding plate and cause an aseismic forearc mantle (Hyndman and Peacock, 2003). These properties entirely justify the lack of seismicity, particularly subduction-related earthquakes, for the shallow portion of the subducted plate along the Manila Trench (Figs. 1 and 4a). As the collisional process is active to the north of these pre-existing fault zones, the free subduction of the southern portion could explain the sinistral movement evidenced by the focal mechanism obtained in this study.

Although recent works have suggested a weakly coupled nature for the northern part of the Manila Trench (e.g., Lin et al., 2015; Doo et al., 2015; Lo et al., 2017), active deformation and thrust fault structures, located in the accretionary wedge and subparallel to the northern Manila Trench have been reported (Lin et al., 2009). Limited by the present observations, it is difficult to know how the principal stress varies from the overriding plate (i.e., the accretionary wedge) to the subducted plate. However, the velocity field derived from the geodetic data indicated a dramatic decrease in magnitude from the east to the west part of Taiwan, implying that a great portion of the convergence rate should be absorbed by the overriding plate (Yu et al., 1997). This feature could provide other evidence for the distinct change in stress on the two sides of the DF.

## 5. Conclusions

A $M_L$ 4.1 earthquake, which occurred on 1 September 2015 near the seismically inactive rifted margin off SW Taiwan, was recorded coincidentally by an OBS network. Analysis of this earthquake series together with the inland CWB seismic station data shows strong evidence for sinistral strike-slip faulting with a dominant plate-motion-parallel tensional stress, which contrasts with the generally accepted belief that a convergent tectonic environment (i.e., Taiwan collision-Manila subduction) is dominated by thrust faulting. The approximately NE-SW rupture direction, which coincides with the pre-existing normal faults generated during the SCS opening phases suggests the possible influence of these pre-existing faults on the regional tectonic context. Fig. 6 shows a 3-D schematic model for the distribution of earthquakes and the possible tectonic environment for the Taiwan collision-Manila subduction transition. The pre-existing normal faults along the passive continental margin (i.e., the northernmost part of the DF) mark an important boundary for the seismicity distribution in the subducted plate. Subduction-related earthquakes could be distinguished only to its south. The abrupt change in seismicity and stress regime shown in our study demonstrates a weak linkage between the collision and subduction portion, which could be generated by a decrease in the lateral connection due to the presence of pre-existing normal faults. Then, the dehydration of the subducted portion causes densification of the subducted plate material and enhances the gravitational slab pull process (black arrow in Fig. 6), which can produce an extensional environment at shallower depths (light arrows in Fig. 6). Since an active collision process exists to the north of the boundary, the oceanward movement of the subducted plate causes the sinistral strike-slip focal mechanism along these transition structures as evidenced in our study by the OBS and inland station data.

Due to the ambiguity of earthquake behaviors and the lack of available data, studies on the Taiwan collision-Manila subduction process could only focus on areas where seismogenic characteristics are typical or discernible. Little knowledge about the transition process was required. Based on the earthquakes and stress distribution, our study shows that the involvement of the pre-existing geological structures could be significant in changing the seismogenic characteristics of the

regional tectonic context, which should be of great importance for estimating the seismic and tsunami potential for the northernmost portion of the SCS. However, it should still be noted that only the seismogenic behaviors in the subducted plate have been discussed in our study. The overriding plate directly receiving the collisional stress from the PSP (i.e., the Luzon Arc) could have more complex seismogenic behaviors, which should be further investigated.

## Acknowledgements

We thank the Geophysical Database Management System (Shin et al., 2013), developed by the Central Weather Bureau (CWB) of Taiwan for providing earthquake catalog. We are especially grateful to Dr. Chien-Hsin Chang for discussion and considerable practical support in data acquisition. All figures were made by the Generic Mapping Tools (Wessel and Smith, 1998). This research was supported by the Central Weather Bureau of Taiwan with grant MOCT-CWB-107-E-05 and by the Ministry of Science and Technology, Taiwan, R.O.C. under Grant no. MOST-107-2116-M-008-017. Two anonymous reviewers are acknowledged for their helpful comments.

## Reference

Allen, R., 1982. Automatic phase pickers: their present use and future prospects. Bull. Seismol. Soc. Am. 72, S225–S242.
Auffret, Y., Pelleau, P., Klingelhoefer, F., Geli, L., Crozon, J., Lin, J.-Y., Sibuet, J.-C., 2004. MicrOBS: a new generation of ocean bottom seismometer. First Break 22, 41–47.
Bent, A.L., 2002. The 1933 Ms = 7.3 Baffin Bay earthquake: strike-slip faulting along the northeastern Canadian passive margin. Geophys. J. Int. 150, 724–736.
Briais, A., Patriat, P., Tapponnier, P., 1993. Updated interpretation of magnetic anomalies and seafloor spreading stages in the South China Sea: Implications for the Tertiary tectonics of Southeast Asia. J. Geophys. Res. 98, 6299–6328.
Brown, D., Wu, Y.-M., Feng, K.-F., Chao, W.-A., Huang, H.-H., 2015. Imaging high-pressure rock exhumation in eastern Taiwan. Geology 43, 651–654.
Chen, Y.R., Lai, Y.C., Huang, Y.L., Huang, B.S., Wen, K.L., 2008. Investigation of source depths of the 2006 Pingtung earthquake sequence using a dense array at teleseismic distances. Terr. Atmos. Ocean. Sci. 19 (6), 579–588.
Chin, S.-J., Lin, J.-Y., Chen, Y.-F., Wu, W.-N., Liang, C.-W., 2016. Transition of the Taiwan-Ryukyu collision-subduction process as revealed by ocean-bottom seismometer observations. J. Asian Earth Sci. 128, 149–157.
Doo, W.-B., Hsu, S.-K., Lo, C.-L., Chen, S.-C., Tsai, C.-H., Lin, J.-Y., Huang, Y.-P., Huang, Y.-S., Chiu, S.-D., Ma, Y.-F., 2015. Gravity anomalies of the active mud diapirs off southwest Taiwan. Geophys. J. Int. 203, 2089–2098.
Eakin, D.H., McIntosh, K.D., Van Avendonk, H., Lavier, L., Lester, R., Liu, C.S., Lee, C.S., 2014. Crustal-scale seismic profiles across the Manila subduction zone: The transition from intraoceanic subduction to incipient collision. J. Geophys. Res. 119, 1–17.
Hsu, Y.-J., Yu, S.-B., Simons, M., Kuo, L.-C., Chen, H.-Y., 2009. Interseismic crustal deformation in the Taiwan plate boundary zone revealed by GPS observations, seismicity, and earthquake focal mechanisms. Tectonophysics 479, 4–18.
Huang, C.-Y., Wu, W.-Y., Chang, C.-P., Tsao, S., Yuan, P.B., Lin, C.-W., Xia, K.-Y., 1997. Tectonic evolution of accretionary prism in the arc-continent collision terrane of Taiwan. Tectonophysics 281, 31–51.
Huang, S.-T., Yang, K.-M., Hung, J.-H., Wu, J.-C., Ting, H.-H., Mei, W.-W., Hsu, S.-H., Lee, M., 2004. Deformation front development at the northeast margin of the Tainan basin, Tainan-Kaohsiung area. Taiwan. Mar. Geophys. Res. 25, 139–156.
Hyndman, R.D., Peacock, S.M., 2003. Serpentinization of the forearc mantle. Earth Planet. Sci. Lett. 212, 417–432.
Institute of Earth Sciences, Academia Sinica, Taiwan, 1996. Broadband array in Taiwan for seismology. Institute of Earth Sciences, Academia Sinica, Taiwan, Other/Seismic Network, doi: 10.7914/SN/TW.
Kao, H., Huang, G.-C., Liu, C.-S., 2000. Transition from oblique subduction to collision in the northern Luzon arc-Taiwan region: Constraints from bathymetry and seismic observations. J. Geophys. Res. 105, 3059. https://doi.org/10.1029/1999J. B900357.
Kennett, B.L.N., Engdahl, E.R., 1991. Traveltimes for global earthquake location and phase identification. Geophys. J. Int. 105, 429–465.
Kirby, S., Engdahl, R.E., Denlinger, R., 1996. Intermediate-depth intraslab earthquakes and arc volcanism as physical expressions of crustal and uppermost mantle metamorphism in subducting slabs. Subduction: top to bottom. In: In: Bebout, G.E. (Ed.), Geophys. Monogr. Ser., vol. 96. AGU, Washington, DC, pp. 195–214.
Kuochen, H., Wu, F.T., Roecker, S.W., 2012. Three-dimensional P velocity structures of the lithosphere beneath Taiwan from the analysis of TAIGER and related seismic data sets. J. Geophys. Res. 117, B06306. https://doi.org/10.1029/2011JB009108.
Lester, R., Van Avendonk, H.J., McIntosh, K., Lavier, L., Liu, C.S., Wang, T., Wu, F., 2014. Rifting and magmatism in the northeastern South China Sea from wide-angle tomography and seismic reflection imaging. J. Geophys. Res. 119, 2305–2323.
Liao, Y.-C., Hsu, S.-K., Chang, C.-H., Doo, W.-B., Ho, M.-Y., Lo, C.-L., Lee, C.-S., 2008. Seismic Tomography off SW Taiwan: A Joint Inversion from OBS and Onshore Data of 2006 Pingtung Aftershocks. Terr. Atmos. Ocean. Sci. 19, 729–741.
Lin, A.T., Yao, B., Hsu, S.-K., Liu, C.-S., Huang, C.-Y., 2009. Tectonic features of the incipient arc-continent collision zone of Taiwan: Implications for seismicity. Tectonophysics 479, 28–42.
Lin, J.-Y., Wu, W.-N., Lo, C.-L., 2015. Megathrust earthquake potential of the Manila subduction system: revealed by the seismic moment tensor element Mrr. Terr. Atmos. Ocean. Sci. 26 (6), 619–630.
Liu, C.-S., Deffontaines, B., Lu, C.-Y., Lallemand, S., 2004. Deformation patterns of an accretionary wedge in the transition zone from subduction to collision offshore southwestern Taiwan. Mar. Geophys. Res. 25, 123–137.
Liu, C.-S., Huang, I.L., Teng, L.S., 1997. Structural features off southwestern Taiwan. Mar. Geol. 137, 305–319.
Lo, C.-L., Doo, W.-B., Kuo-Chen, H., Hsu, S.-K., 2017. Plate coupling across the northern Manila subduction zone deduced from mantle lithosphere buoyancy. Phys. Earth Planet. In. 273, 50–54.
McIntosh, K., Lavier, L., van Avendonk, H., Lester, R., Eakin, D., Liu, C.-S., 2014. Crustal structure and inferred rifting processes in the northeast South China Sea. Mar. Pet. Geol. 58, 612–626.
McIntosh, K., van Avendonk, H., Lavier, L., Lester, W.R., Eakin, D., Wu, F., Liu, C.-S., Lee, C.-S., 2013. Inversion of a hyper-extended rifted margin in the southern Central Range of Taiwan. Geology 41, 871–874.
Rau, R.-J., Lee, J.-C., Ching, K.-E., Lee, Y.-H., Byrne, T.B., Chen, R.-Y., 2012. Subduction-continent collision in southwestern Taiwan and the 2010 Jiashian earthquake sequence. Tectonophysics 578, 107–116.
Reed, D.L., Lundberg, N., Liu, C.-S., Kuo, B.-Y., 1992. Structural relations along the margins of the offshore Taiwan accretionary wedge: implications for accretion and crustal kinematics. Acta Gelol. Taiwanica 105–122.
Seno, T., Stein, S., Gripp, A.E., 1993. A model for the motion of the Philippine Sea Plate consistent with NUVEL-1 and geological data. J. Geophys. Res. 98, 17941–17948.
Shin, T.-C., Chang, C.-H., Pu, H.-C., Lin, H.-W., Leu, P.-L., 2013. The geophysical Database management system in Taiwan. Terr. Atmos. Ocean. Sci. 24, 11–18.
Shyu, J.B.H., Sieh, K., Chen, Y.G., Liu, C.S., 2005. Neotectonic architecture of Taiwan and its implications for future large earthquakes. J. Geophys. Res. 110. https://doi.org/10.1029/2004JB003251.
Suppe, J., 1984. Kinematics of arc-continental collision, flipping of subduction and back-arc spreading near Taiwan. Mem. Geol. Soc. China 6, 21–33.
Talwani, P., Rajendran, K., 1991. Some seismological and geometric features of intraplate earthquakes. Tectonophysics 186, 19–41.
Taylor, B., Hayes, D.E., 1983. Origin and history of the South China Sea basin. Tectonic Geol. Evol. Southeast Asian Seas Islands: Part 2, 23–56.
Teng, L.S., 1990. Geotectonic evolution of late Cenozoic arc-continent collision in Taiwan. Tectonophysics 183, 57–76.
Tsai, Y., Teng, T., Chiu, J., Liu, H., 1977. Tectonic implications of the seismicity in the Taiwan region. Mem. Geol. Soc. China 2, 13–41.
Waldhauser, F., Ellsworth, W.L., 2000. A double-difference earthquake location algorithm: Method and application to the northern Hayward fault. California. Bull. Seismol. Soc. Am. 90, 1353–1368.
Wessel, P., Smith, W.H., 1998. New, improved version of Generic Mapping Tools released. Eos, Trans. Amer. Geophys. Union 79 (47), 579. https://doi.org/10.1029/98EO00426.
Wu, Y.-M., Chang, C.H., Zhao, L., Teng, T.L., Nakamura, M., 2008. A Comprehensive Relocation of Earthquakes in Taiwan from 1991 to 2005. Bull. Seismol. Soc. Am. 98, 1471–1481.
Wu, Y.-M., Hsu, Y.-J., Chang, C.-H., Teng, L.S., Nakamura, M., 2010. Temporal and spatial variation of stress field in Taiwan from 1991 to 2007: Insights from comprehensive first motion focal mechanism catalog. Earth Planet. Sci. Lett. 298, 306–316.
Wu, Y.-M., Zhao, L., Chang, C.-H., Hsiao, N.-C., Chen, Y.-G., Hsu, S.-K., 2009. Relocation of the 2006 Pingtung earthquake sequence and seismotectonics in Southern Taiwan. Tectonophysics 479, 19–27.
Yang, K.-M., Huang, S.-T., Wu, J.-C., Ting, H.-H., Mei, W.-W., 2006. Review and new insights on foreland tectonics in western Taiwan. Int. Geol. Rev. 48, 910–941.
Yang, K.-M., Rau, R.-J., Chang, H.-Y., Hsieh, C.-Y., Ting, H.-H., Huang, S.-T., Wu, J.-C., Tang, Y.-J., 2016. The role of basement-involved normal faults in the recent tectonics of western Taiwan. Geol. Mag. 153, 1166–1191.
Yeh, Y.-C., Hsu, S.-K., Doo, W.-B., Sibuet, J.-C., Liu, C.-S., Lee, C.-S., 2012. Crustal features of the northeastern South China Sea: insights from seismic and magnetic interpretations. Mar. Geophys. Res. 33, 307–326.
Yu, H.-S., 2004. Nature and distribution of the deformation front in the Luzon Arc-Chinese continental margin collision zone at Taiwan. Mar. Geophys. Res. 25, 109–122.
Yu, S.-B., Chen, H.-Y., Kuo, L.-C., 1997. Velocity field of GPS stations in the Taiwan area. Tectonophysics 274, 41–59.
Zhao, M., Qiu, X., Xia, S., Xu, H., Wang, P., Wang, T.-K., Lee, C.-S., Xia, K., 2010. Seismic structure in the northeastern South China Sea: S-wave velocity and Vp/Vs ratios derived from three-component OBS data. Tectonophysics 480, 183–197.